Surface Composition Effects in Electrocatalysis: Kinetics of Oxygen Reduction on Well-Defined Pt_3Ni and Pt_3Co Alloy Surfaces

V. Stamenković,* T. J. Schmidt, P. N. Ross, and N. M. Marković

Materials Sciences Division, Lawrence Berkeley National Laboratory, University of California at Berkeley, Berkeley, California 94720

Received: May 9, 2002; In Final Form: August 23, 2002

The oxygen reduction reaction (ORR) has been studied on polycrystalline Pt_3Ni and Pt_3Co alloys in acid electrolytes using the rotating ring disk electrode (RRDE) method. Preparation and characterization of alloy surfaces were performed in ultrahigh vacuum (UHV). Clearly defined surface composition was determined via low-energy ion-scattering (LEIS) spectroscopy. Polycrystalline bulk alloys of Pt_3Ni and Pt_3Co were prepared in UHV having two different surface compositions: one with 75% Pt and the other with 100% Pt. The latter we call a "Pt-skin" structure and is produced by an exchange of Pt and Co in the first two layers. The base voltammetry in 0.1 M $HClO_4$ solution of the 75% Pt alloy surface indicated a decrease of H_{upd} pseudocapacitance (ca. 30−40 $\mu C/cm^2$) consistent with the surface composition determined in UHV. With the exception of the "Pt-skin" surface on Pt_3Ni, all the alloy electrodes exhibited stable $i-E$ curves with repeated cycling between 0.05 and 1.0 V at all temperatures. Activities of Pt-alloys for the ORR were compared to the polycrystalline Pt in 0.5 M H_2SO_4 and 0.1 M $HClO_4$ electrolytes in the temperature range of $293 < T < 333$ K. It was found that the order of activity is dependent on the nature of anions of supporting electrolytes: in H_2SO_4 the activity increased in the order $Pt_3Ni > Pt_3Co > Pt$; in $HClO_4$, however, the order of activities at 333 K was "Pt-skin" > $Pt_3Co > Pt_3Ni > Pt$. The catalytic enhancement was greater in 0.1 M $HClO_4$ than in 0.5 M H_2SO_4, with the maximum enhancement observed for the "Pt-skin" on Pt_3Co in 0.1 M $HClO_4$ being 3−4 times that for pure Pt. Catalytic enhancement of the ORR on Pt_3Ni and Pt_3Co vs Pt was attributed to the inhibition of $Pt-OH_{ad}$ formation on Pt sites surrounded by "oxide" covered Ni and Co atoms beyond 0.8 V. Kinetic analyses of RRDE data revealed that kinetic parameters for the ORR and the production of H_2O_2 on the Pt_3Ni, Pt_3Co, and "Pt-skin" alloys are the same as on pure Pt: reaction order, $m = 1$, two identical Tafel slopes in $HClO_4$, and a single Tafel slope in H_2SO_4, apparent activation energy $\approx$ 21−25 kJ/mol. The fact that essentially the same kinetic parameters are assessed from the analysis of the ORR data on all three surfaces implies that the reaction mechanism on Pt_3Ni and Pt_3Co alloy surfaces is the *same* as one proposed for pure Pt, i.e., a "series" $4e^-$ reduction pathway.

1. Introduction

In the past few years, considerable progress has been made in the understanding of the ORR on Pt and Pt-bimetallic surfaces.[1] To this end, variations of metal surface crystallography and/or electronic properties by intermixing two or more metals have often been employed to delineate very important electrocatalytic trends. For example, it was demonstrated that the kinetics of the ORR on Pt(*hkl*) varies with the crystal face in a different manner depending on the electrolyte, suggesting that dependence of surface geometry arises primarily due to structure-sensitive adsorption of specifically adsorbing anions.[1−5] To probe the electronic effects, the ORR kinetics was investigated on thin metal films grown epitiaxially on foreign metal substrates.[6,7] Several investigations have been carried out to determine the role of alloying in the electrocatalytic activity of Pt for the ORR.[8−16] It is unclear, however, whether there is any alloy of Pt that is more active than Pt itself. With an exception of work by Toda et al.,[15] most of the studies reporting improved activity have been done on supported catalysts, where the kinetic measurements themselves are subject to considerable uncertainty.[16,17] One of the difficulties in determining the effect of alloying components using supported catalysts is that the activity of supported catalysts can have a wide range of values, depending on their microstructure and/or method of preparation. Since the alloyed Pt catalyst particles may not have either the same particle size or shape as the Pt catalysts to which they are compared, a simple comparison of activity normalized either by mass or surface area is insufficient to identify a true alloying effect. Furthermore, to get insight into the relationship between the surface composition and the catalytic activity, it is very important to determine if the surface segregation takes place during the preparation of bimetallic surfaces, i.e., enrichment of one element at the surface relative to the bulk.[1,18−21] The details of segregation are still not completely understood, especially in the case of segregation of nanoparticles which may differ from that of their bulk analogue.[22,23] This is not surprising, considering that nanoclasters represent a finite quantity of material, so there is no infinite source/sink of constituent atoms and hence material balance constraints become important. Clearly, all of these complexities on high-surface area bimetallic catalysts reinforce the need for using well-characterized materials to identify the fundamental mechanisms at work in the electrocatalysis of the ORR.

In this paper, the intrinsic catalytic activity of Pt_3Ni and Pt_3Co alloy catalysts for the ORR are studied on UHV-prepared (annealing/sputtering cycles) and characterized (AES and LEIS)

* Corresponding author. E-mail: vrstamenkovic@lbl.gov.

10.1021/jp021182h CCC: $22.00
Published on Web 10/26/2002

alloys in acid electrolytes. Emphasis will be placed on the description of alloy surface preparation and the characterization procedure as well as on kinetic studies of the ORR. It will be demonstrated that the ability to make a controlled and well-characterized arrangement of two elements in the electrode surface region is essential to interpreting the kinetic results.

2. Experimental Section

2.1. Surface Preparation and Characterization. The polycrystalline bulk Pt−Ni and Pt−Co alloy electrodes used in this study were prepared by conventional metallurgy. Bulk composition ($x_{Ni(Co),b}$) was assessed via X-ray fluorescence spectroscopy ($x_{Ni(Co),b} \approx 0.75$); X-ray diffraction showed all specimens to be single-phase *fcc* solid solutions of Pt and Ni(Co) having the expected lattice constant for 75% Pt.[24] Cleaning, modification, and surface characterization procedure were performed in a UHV system, under base pressure of 2×10^{-10} Torr range, which is equipped with an angular-resolving double pass cylindrical mirror analyzer PHI-DPCMA F15-255GAR with an electron source at its center. The UHV cleaning procedure was done by repeating of sputtering−annealing cycles with Ar^+ and oxygen until Auger electron spectroscopy (AES) indicated that a perfectly clean (carbon and oxygen-free) surface was produced. AES spectra were recorded in derivative mode using the 3 keV electron beam energy, 3 eV_{p-p} modulation, and −5 μA beam current in the range from 140 to 900 eV.

To produce a different surface composition, clean samples were either annealed at 1000 K or mildly sputtered with a 0.5 keV beam of Ar^+ ions. The surface composition of alloy samples was determined by low-energy ion-scattering (LEIS) spectroscopy. A compilation of surfaces analyzed by LEIS spectroscopy has been made by Watson.[25] LEIS spectra were taken with He^+ and Ne^+ beam energy of 1 keV with sample current from 5 to 30 nA at residual He/Ne pressure of 2.5×10^{-8} Torr. The scattering angle was 127°, and the incidence angle was 45°. A Φ04-303A differentially pumped ion gun was used to raster a He^+ or Ne^+ ion beam over approximately a 3 mm × 3 mm area. Time of recording was 60 s/spectrum. The clean Pt reference sample was prepared in the same manner i.e., conventional metallurgy and pretreated in UHV in exactly the same way, mild sputter cleaning and/or annealing.

2.2. Electrochemical Measurements. The UHV-prepared and characterized alloy surfaces were withdrawn form the UHV introductory port (back-filled with argon) into air and covered immediately with a drop of triply pyro-distilled water; for details, see ref 26. The electrodes were then mounted in a rotating ring disk electrode and finally immersed in electrolyte under potential control at ∼0.05 V vs RHE in 0.5 M H_2SO_4 (Baker, Ultrex) and 0.1 M $HClO_4$ (Baker, Ultrex). Electrolytes were prepared with triple pyro-distilled water and thermostated at 293, 303, 313, and 333 K, by circulating constant-temperature bath connected with the water jacket of a standard three-compartment electrochemical cell. The reference electrode was a saturated calomel electrode (SCE) separated by a bridge from the reference compartment. All potentials in this paper are, however, referenced to the reversible hydrogen electrode potential (RHE) at the same temperature (calibrated from hydrogen oxidation reaction [27]) in the same electrolyte; argon, oxygen, and hydrogen were bubbled through a glass frit (Air Products, 5N8 purity). During measurement of the polarization curves for the ORR on the disk electrode, the ring electrode was potentiostated at 1.15 V, a potential where the peroxide oxidation reaction is under pure diffusion control; collection efficiency (N) for the ring-disk assembly is ca. 0.2. The geometrical surface area of the disk electrode was 0.283 cm^2, and all voltammograms were recorded with a sweep rate of either 50 or 20 mV/s.

3. Results and Discussion

3.1. Surface Composition. The relation between the surface and the bulk composition of alloys has been the subject of intensive research, in both theory and experiment.[28−32] For example, surface enrichment of Au is always detected for $Au_3Pd(100)$,[33] $Au_3Pd(110)$,[34] and $Cu_3Au(111)$[35] alloy surfaces. According to UHV studies, $Pt_{78}Ni_{22}(111)$,[36] $Pt_{80}Co_{20}(001)$,[37] and $Pt_{80}Co_{20}(111)$[38] alloys exhibit highly structured compositional oscillations in the first three atomic layers. The studies revealed that, for the (111) and (100) crystals, the outermost layer of the clean, annealed surfaces is *pure* Pt, which we shall call hereafter the "skin" structure, with Pt depletion in the second layer. It has been found that at least some catalytic properties of the "Pt-skin" structures in UHV are different from the pure Pt surface.[18,37] This was attributed to the electronic effect of intermetallic bonding of the Ni(Co)-rich second layer with the topmost Pt atoms. As we demonstrate below, the "skin" structure with a characteristic catalytic activity can also be created on polycrystalline Pt_3Ni and Pt_3Co alloys.

The AES and LEIS spectra of Pt_3Ni and Pt_3Co polycrystalline samples, obtained after either mild sputtering or annealing of specimens, are shown in Figures 1 and 2. The AES reveal that, after sputtering/annealing cycles, both alloy surfaces were clean, showing characteristic Pt (158, 168, 189, 199, 237, 251, 390 eV) and Ni (716, 783, 848 eV) (Figure 1a) or Pt and Co (656, 716, 775 eV) (Figure 1a and 2a) peaks. Quantitative surface analysis of the Pt−Ni(Co) alloy with AES is quite complicated, requiring modeling of emission from several subsurface layers with dynamical scattering of the outgoing Auger electron. Because the contribution of Auger emission from the several atomic layers in the Pt_3−Ni(Co) alloy causes the Pt/Ni(Co) AES ratio to be much different than the ratio would be with emission only from the first layer, AES has been used only to verify the cleanliness of alloy surfaces. In contrast, the true surface composition of the outermost atomic layer of the Pt_3−Ni(Co) alloy can be obtained by utilizing LEIS, as shown in Figures 1b and 2b. The scattering peaks of the Pt and Ni(Co) are calculated from the classical equation for elastic collisions.[39] The data, obtained by a 1 keV Ne^+ beam, show that the first layer of a clean annealed Pt_3−Ni(Co) surface contains only Pt atoms, implying that the "Pt-skin" structure can also be created on a polycrystalline $Pt_3Ni(Co)$ alloy. The LEIS spectra taken after mild sputtering unambiguously show that Ni(Co) are indeed present in the outermost layer of the clean sputtered surface. Using the elemental sensitivity factors of polycrystalline materials,[40] surface composition is estimated to be 75% of Pt and 25% of Ni/Co, equal to the bulk concentration of Pt_3Co and Pt_3Ni alloys (denoted hereafter as Pt_3Ni and Pt_3Co). As mentioned above, both annealed and mildly sputtered specimens were transferred into the electrochemical cell for further electrochemical characterization.

3.2. Cyclic Voltammetry. The corresponding cyclic voltammograms of mildly sputtered Pt, Pt_3Ni, Pt_3Co, and "Pt-skin" electrodes recorded immediately following transfer from UHV in argon-purged 0.1 M $HClO_4$ and 0.5 M H_2SO_4 at 293 K are shown in Figures 1c and 2c. Voltammetry shows three characteristic potential regions: the hydrogen adsorption potential region (denoted hereafter as the underpotentially deposited hydrogen, H_{upd}, $0 < E < 0.35$ V), in which H_{upd} adsorption/desorption is accompanied by desorption/adsorption of anions of the supporting electrolyte, is followed first by the double

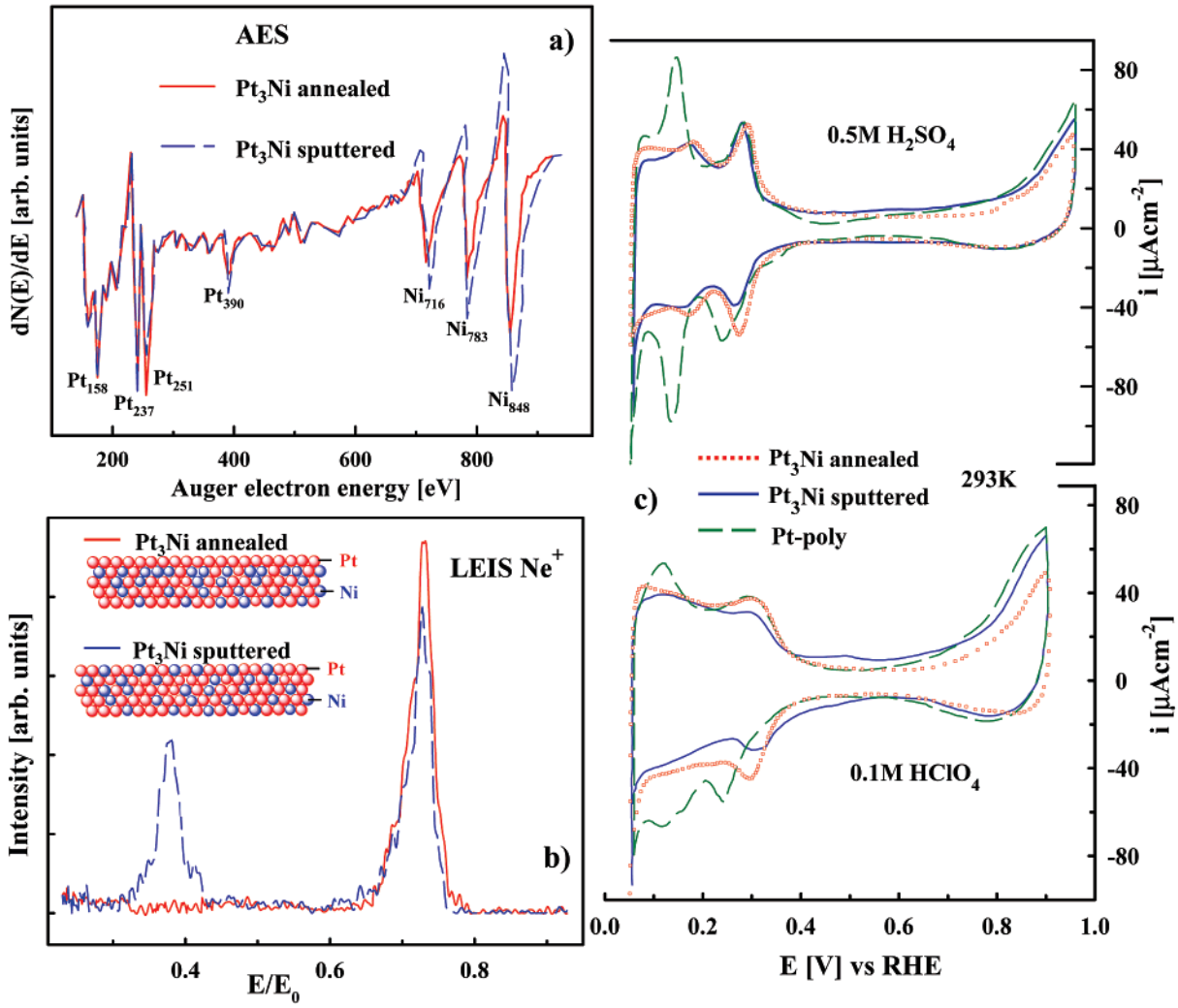

Figure 1. (a) Auger electron spectroscopy of annealed and mildly sputtered Pt_3Ni. (b) Low-energy ion-scattering spectra of the same two surfaces. Also shown is a schematic picture of the "Pt-skin" electrode and the sputtered Pt_3Ni electrode. (c) Cyclic voltammetry (50mV/s) of Pt and two Pt_3Ni surfaces at 295 K in 0.5 M H_2SO_4 (upper curves) and 0.1 M $HClO_4$ (lower curves).

layer potential region (ca. $0.4 < E < 0.7$ V) and then by the oxide formation potential region, $E >$ ca. 0.7 V. As shown in Figures 1c and 2c, both the H_{upd} features as well the oxide formation on Pt are strongly affected by the nature of anions; e.g., in contrast to relatively broad H_{upd} peaks in $HClO_4$, two sharp H_{upd} peaks are observed in H_2SO_4, and the surface coverage by oxide is reduced in the latter electrolyte. These experimental observations for pure Pt are not new, and they are consistent with the recent theoretical calculations that for polyatomic oxyanions the Pt-anion strength of interaction is mostly determined by the different degrees of back-donation to the empty levels of the anions, being more pronounced for $Pt-HSO_4^-$ than for $Pt-ClO_4^-$ interaction.[41] Figures 1c and 2c show that although voltammograms of the sputtered Pt_3Ni and Pt_3Co alloys are very similar to that for the sputtered Pt surface, the distribution of charge under the peaks in the H_{upd} potential region is characteristically different, i.e., there is less charge under the peak near 0.1 V and more under the peak near 0.3 V on the alloy surfaces. Assuming that neither Ni nor Co are active sites for adsorption of hydrogen, the difference in the distribution of charge in the H_{upd} potential region between Pt and Pt alloys arises due to the lack of adsorption of H_{upd} on alloying components. Of greater importance is the comparison of voltammetry between the sputtered alloy surfaces and annealed surfaces having the "Pt-skin" structure. Here it is easily seen that the total charge in the H_{upd} region on the alloy surfaces increases upon annealing, consistent with the increase in surface concentration of Pt. Quantitatively, the increase is slightly less than the 25% increase in Pt surface concentration (from ca. 165 to 200 $\mu C/cm^2$), but the differences in double-layer capacitance at ca. 0.5 V are consistent with an expected decrease in surface roughness upon annealing, so that the Pt atom density would be somewhat less than 25%. A close inspection of Figure 1 also indicates that, on the Pt_3Ni and Pt_3Co alloys, the onset of oxide formation shifts toward more positive potentials, suggesting that alloying with Ni(Co) effects a fundamental change in the way Pt atoms interact with H_2O and anions of supporting electrolytes.

It is important to note that the base voltammetry of all four electrodes recorded above room temperature (not shown) are very similar to those observed at 293 K. These results are in accordance with the previous observation that temperature (in the range of 293−333 K) has a rather small effect on the voltammetric features of polycrystalline Pt and Pt single crystals in acid[27,42] and alkaline[43] solutions. It is also important to emphasize that, except from the "Pt-skin" structure for the Pt_3Ni alloy, all voltammetric features shown in Figures 1c and 2c were reproduced in the subsequent scans. The base voltammetry remained stable even at elevated temperature ($293 < T < 333$ K), implying that during the duration of the experiment

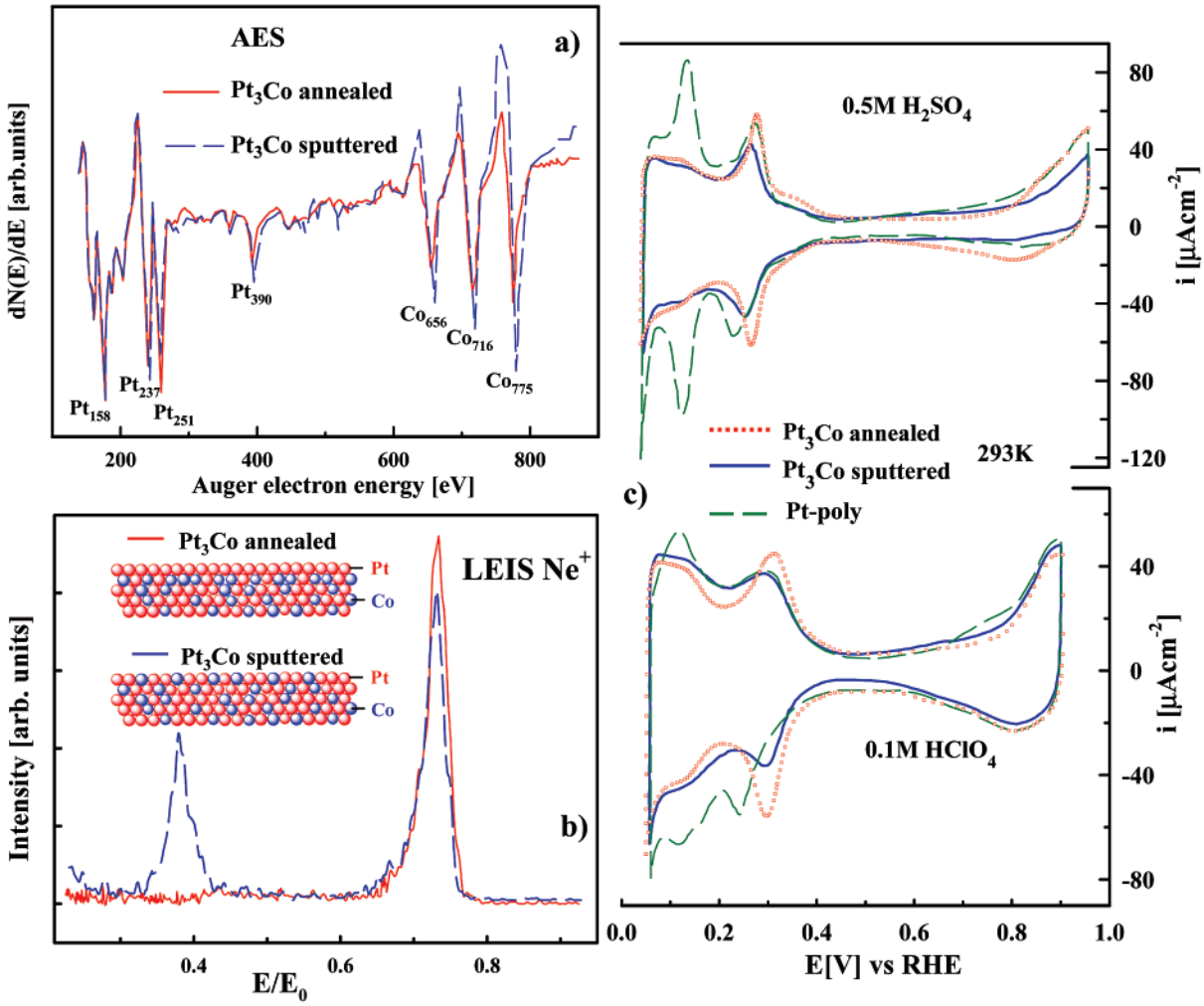

Figure 2. (a) Auger electron spectroscopy of annealed and mildly sputtered Pt_3Co. (b) Low-energy ion-scattering spectra of the same two surfaces. Also shown is a schematic picture of the "Pt-skin" electrode and the sputtered Pt_3Co electrode. (c) Cyclic voltammetry (50mV/s) of Pt and two Pt_3Co surfaces at 295 K in 0.5 M H_2SO_4 (upper curves) and 0.1 M $HClO_4$ (lower curves).

(including the measurements of ORR kinetics) there is no corrosion/dissolution of alloying components. However, the voltammetry for the Pt-skin structure of the Pt_3Ni alloy was not stable to potential cycling in the region shown and, for that reason, we will not present the ORR kinetic results with that sample.

3.3. Oxygen Reduction Kinetics. For the purpose of demonstrating the methodology of probing the kinetic activity of Pt_3Ni and Pt_3Co alloys, a representative set of polarization curves for the ORR on the sputtered Pt_3Co alloy in 0.1 M $HClO_4$ at 298 K along with the kinetic analyses, presented in the form of the Tafel plot (insert b) of mass-transport corrected currents (see eq 2) and the Levich-Kotecky plots (insert c), are shown in Figure 3. Well-defined diffusion limiting currents (i_D) for the ORR (0.2 to 0.7 V) are followed by a mixed kinetic-diffusion control between $0.8 < E < 1.0$ V. Figure 3 also shows that in both potential regions the ring currents (I_R) are a small fraction of i_D, implying that the ORR proceeds almost entirely through a $4e^-$ reduction pathway. The appearance of the peroxide oxidation currents parallels the adsorption of hydrogen on the Pt_3Co electrode ($E < 0.2$ V), reaching the maximum of ca. 20% at 0.075 V. Quantitative representation of the peroxide production (current efficiency) was calculated from eq 1:[44]

$$x_{H_2O_2} = \frac{2I_R/N}{i_D + I_R/N} \qquad (1)$$

where N is the collection efficiency of the ring-disk electrode. As mentioned above, in subsequent potential cycles, both i_D and I_R remain the same, confirming that the surface composition of alloys remains the same during the ORR experiments.

Figure 3b shows the Tafel plot which is assessed from the potentiodynamic measurements illustrated in Figure 3a. The polarization curve was fitted somewhat arbitrarily with two tangents through the points of what appear to be a continuous curve. This corresponds to two Tafel slopes; ca. 74 mV/dec for $E < 0.86$ V and ca. 113 mV/dec for $E > 0.86$ V. As will be discussed in Section 3.4, the transition in the Tafel slope appears to be related to the change in the nature of oxygen-containing species with potential, a transition that strongly affects the ORR.[4,45−49] Figure 3c shows the so-called Levich-Kautecky plot, eq 2:

$$\frac{1}{i} = \left(\frac{1}{i_k} + \frac{1}{i_d}\right) = f(\omega^{-1/2})_E \qquad (2)$$

where for various potentials yields (E) and applied rotational rates (ω), each straight line intercept corresponds to the kinetic current, i_k. Notice that intercept gives the order of absolute kinetic activity of the Pt_3Co surface for the ORR. In addition, the slope of the straight lines, the so-called "B-factor", allows one to assess the number of electrons involved in the oxygen reduction reaction. The experimental value of ca. 4.28×10^{-2}

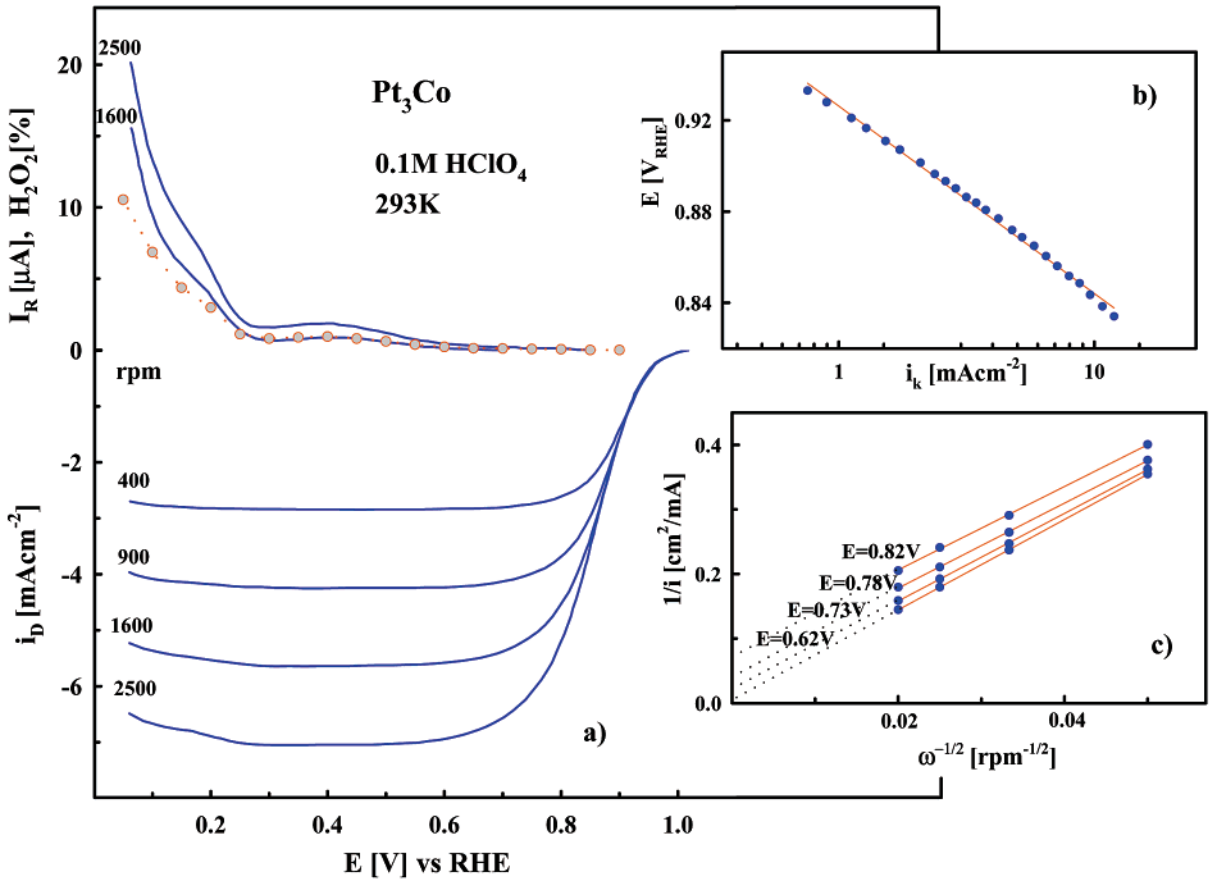

Figure 3. (a) Disk (i_D) and ring (I_R) currents (anodic sweep direction) during the ORR on mildly sputtered Pt_3Co in 0.1 M $HClO_4$ at a sweep rate of 20 mV/s; Ring potential, $E = 1.15$ V; Collection efficiency: $N = 0.2$. (b) Tafel plot at 1600 rpm. (c) Levich plot at various electrode potentials.

mA rpm$^{0.5}$ obtained from Figure 3c is in excellent agreement with the theoretical value of 4.27×10^{-2} mA rpm$^{0.5}$, calculated for the four-electron process from the Levich equation,[50] using literature data for oxygen solubility,[51,52] c_0 ($c_0 = 1.26 \times 10^{-3}$ mol L^{-1}), oxygen diffusivity,[53] D ($D = 1.93 \times 10^{-5}$ cm^2 s^{-1}), and kinematic viscosity of the electrolyte,[51] ν ($\nu = 1.009 \times 10^{-2}$ cm^2 s^{-1}). The linearity of the plots in Figure 3c implies a first-order dependence of O_2 kinetics on the Pt_3Co alloy (25% Co). Since the measurements of the kinetics as a function of partial pressure of O_2 are not available, the reaction order (m) was checked further from log i vs log[$i - i_d/i_d$] functionality (not shown) using data from Figure 3c; for details see ref 43. The value of $m = 1.09$ was obtained, confirming first-order dependence of the kinetics of ORR on the Pt_3Co surface. A very similar relationship is observed for the plots in sulfuric acid solution, and thus the later results are not shown. All important kinetic parameters, however, obtained by using the same methodology as described above, for the ORR on Pt, sputtered Pt_3Ni(Co), and the "Pt-skin" Pt_3Co electrode in 0.1 M $HClO_4$ and 0.5 M H_2SO_4 at two temperatures are listed in Table 1.

Potentiodynamic polarization curves for 75% Pt alloy surfaces are shown for the ORR first in 0.1 M $HClO_4$ (Figure 4) and then in 0.5 M H_2SO_4 (Figure 5). Corresponding curves for the pure Pt in both electrolytes are also shown as a reference. A close inspection of Figures 4 and 5 reveals that the reaction rates on Pt, Pt_3Ni, and Pt_3Co are much higher in $HClO_4$ than in H_2SO_4. Furthermore, the order of activity is also dependent on the supporting electrolyte. For example, in $HClO_4$, Pt_3Co is more active than Pt_3Ni, while in H_2SO_4, Pt_3Ni is the most active electrode. The fact that activities are significantly higher in

TABLE 1: Kinetic Parameters for the ORR on Pt and Pt Bimetallic Surfaces in 0.1 M $HClO_4$ and 0.5 M H_2SO_4[a]

0.1 M $HClO_4$

	$\partial E/\partial \log(i_k)$ [mV/dec]		$\Delta H^{\#}$		
	293 K	333 K	[kJ mol^{-1}]		
electrode	lcd/hcd	lcd/hcd	@$\eta = 0.30$ V	m	n
Pt (pc)	81/112	67/87	21	1	4
Pt_3Ni-sputtered	86/113	54/78	23	1	4
Pt_3Co-sputtered	74/107	55/77	22	1	4
Pt_3Co-annealed	81/105	61/77	25	1	4

0.5 M H_2SO_4

	$\partial E/\partial \log(i_k)$ [mV/dec]			
electrode	293 K	333 K	m	n
Pt (pc)	128	136	1	4
Pt_3Ni-sputtered	125	130	1	4
Pt_3Co-sputtered	118	131	1	4

[a] $\partial E/\partial \log(i_k)$: Tafel slope; lcd/hcd: low/high current density; ΔH: activation energy; m: reaction order; n: number of electrons.

$HClO_4$ than in H_2SO_4, i.e., the same electrode is always less active in H_2SO_4 than in $HClO_4$, suggests that bisulfate adsorption on Pt sites inhibits the reduction by blocking the initial adsorption of O_2 [3], but it does not affect the reaction pathway, since no H_2O_2 is detected on the ring electrode in the kinetically controlled potential region. Figures 4a and 5a show that H_2O_2 is also not detected during the ORR on Pt_3Co and Pt_3Ni electrodes in both electrolytes. In fact, in the potential region of $0.05 < E < 1$ V, similarly small amounts of H_2O_2 are detected on the ring electrode on all three surfaces at 293 K, implying that, even though Pt_3Co and Pt_3Ni electrodes are more

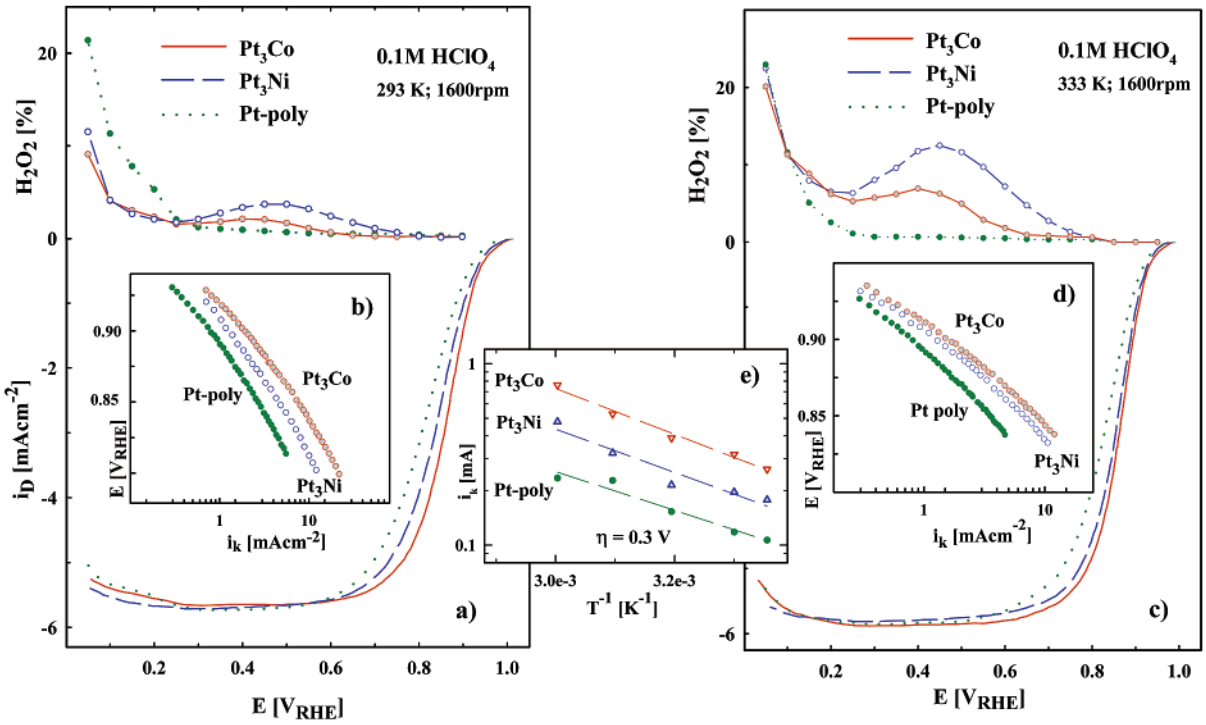

Figure 4. (a) Disk (i_D) and ring (I_R) currents (anodic sweep direction) during the ORR on mildly sputtered Pt, Pt_3Co, and Pt_3Ni in 0.1 M $HClO_4$ at 293 K. Insert b: Tafel plots for all three surfaces at 293 K. (c) Disk (i_D) and ring (I_R) currents (anodic sweep direction) during the ORR on mildly sputtered Pt, Pt_3Co, and Pt_3Ni in 0.1 M $HClO_4$ at 333 K. Insert d: Tafel plots for all three surfaces at 333 K. Sweep rate: 20 mV/s; Ring potential, $E = 1.15$ V; Collection efficiency: $N = 0.2$. Insert e: Arrhenius plots at overpotential of 0.3 V for the ORR on Pt, Pt_3Co, and Pt_3Ni electrodes.

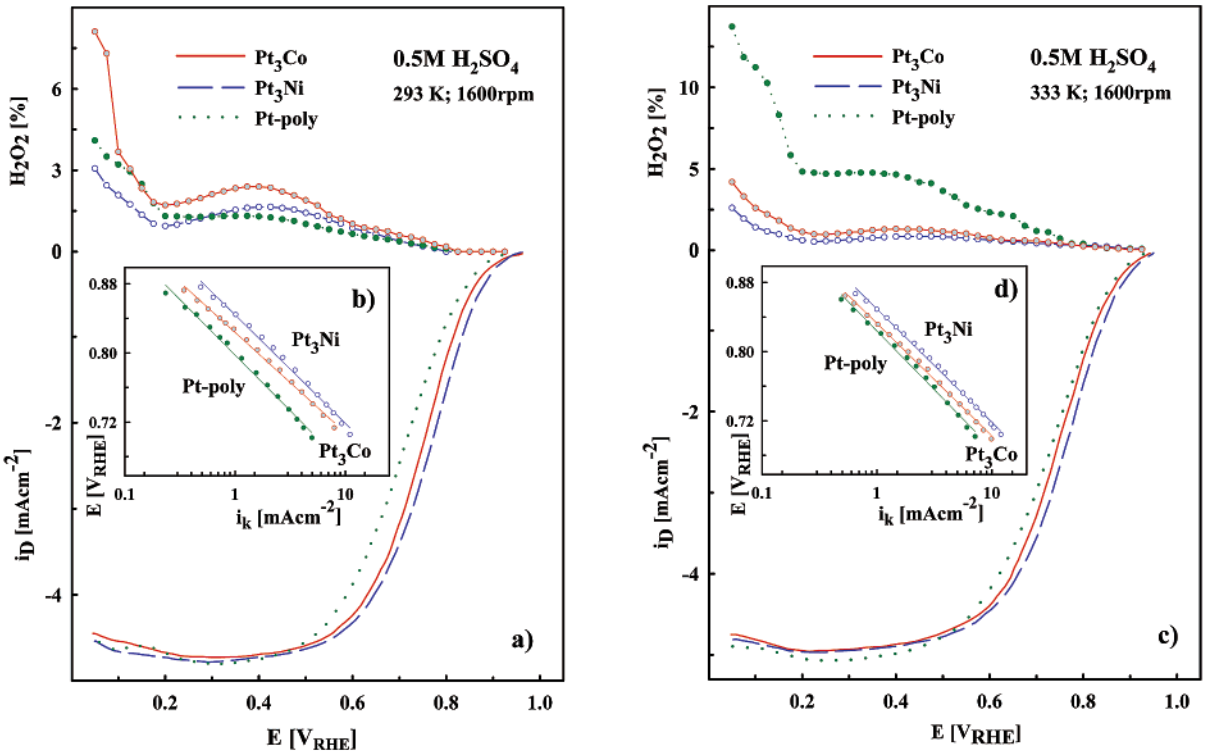

Figure 5. (a) Disk (i_D) and ring (I_R) currents (anodic sweep direction) during the ORR on mildly sputtered Pt, Pt_3Co, and Pt_3Ni in 0.5 M H_2SO_4 at 293 K. Insert b: Tafel plots for all three surfaces at 293 K. (c) Disk (i_D) and ring (I_R) currents (anodic sweep direction) during the ORR on mildly sputtered Pt, Pt_3Co, and Pt_3Ni in 0.5 M H_2SO_4 at 333 K. Insert d: Tafel plots for all three surfaces at 333 K. Sweep rate: 20 mV/s; Ring potential, $E = 1.15$ V; Collection efficiency: $N = 0.2$.

active than Pt, the reaction pathway of the ORR on Pt alloys may be the same as for a pure Pt electrode. At higher temperatures (Figures 4b and 5b), the polarization curves are qualitatively similar to the curves recorded at room temperature, having the same order of activity as at 293 K.

The results for the ORR on the "Pt-skin" electrode (annealed surface) in 0.1 M $HClO_4$ are shown in Figure 6. Clearly, at 333 K, the "Pt-skin" structure is more active than both pure Pt and 75% Pt−25% Co alloy surface (insert of Figure 6), suggesting that a uniform monatomic layer of Pt surface atoms, with Pt

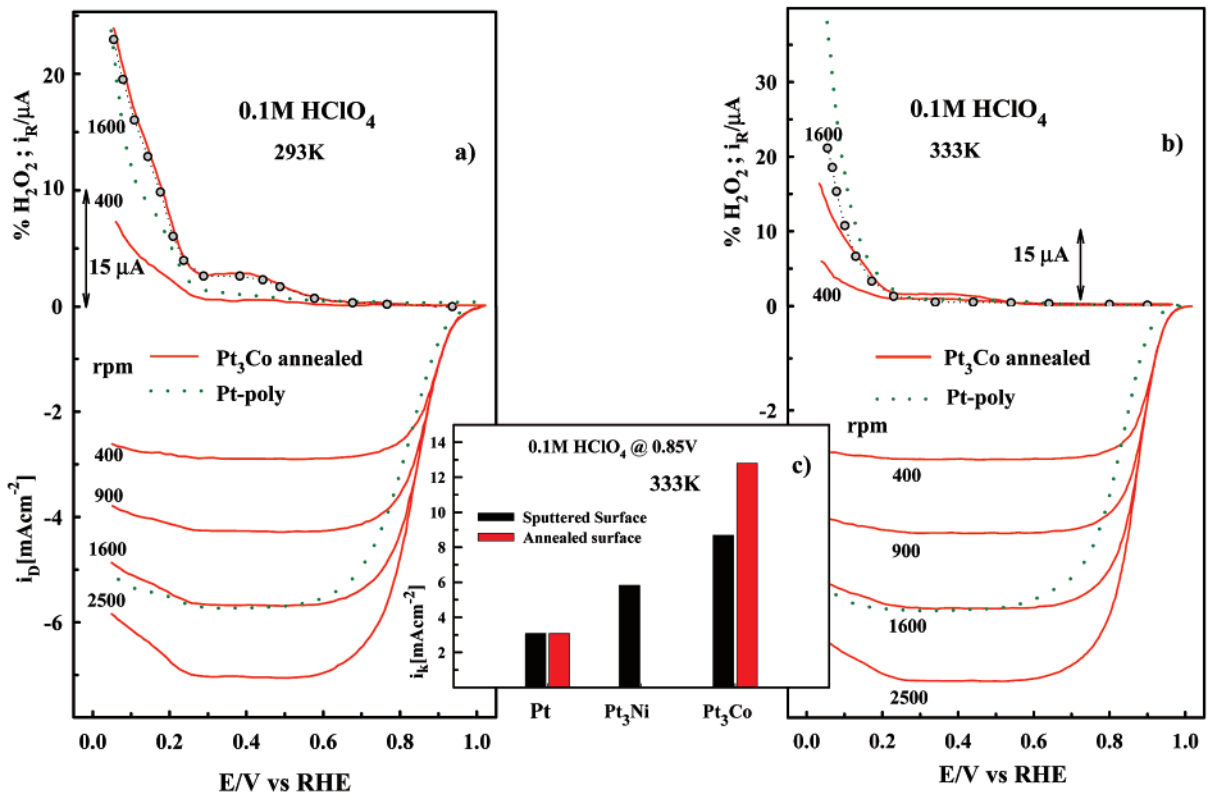

Figure 6. (a) Disk (i_D) and ring (I_R) currents (anodic sweep direction) during the ORR on UHV-annealed Pt and Pt_3Co electrodes in 0.1 M $HClO_4$ at 293 K. Insert b: Tafel plots for these two surfaces at 293 K. (c) Disk (i_D) and ring (I_R) currents (anodic sweep direction) during the ORR on UHV-annealed Pt and Pt_3Co electrodes in 0.1 M $HClO_4$ at 333 K. Insert d: Tafel plots these two surfaces at 333 K. Sweep rate: 20 mV/s; Ring potential, $E = 1.15$ V; Collection efficiency: $N = 0.2$. Insert e: Histograms showing the kinetic currents densities at $E = 0.85$ V for the catalysts in this study obtained at 333 K.

depletion and Co enrichment in the second layer, has unique catalytic properties. These results show that the kinetics of the ORR are dependent not only on the nature of alloying component (Pt < Pt_3Ni < Pt_3Co) but also on the exact arrangement of the alloying element in the surface region (Pt_{bulk} < Pt_3Co < "Pt-skin" on Pt_3Co).

The effect of temperature on the rate of the ORR is clearly visible in Figures 4 and 5. As expected, the kinetics of the ORR is higher at elevated temperatures, reflecting the temperature dependence of the chemical rate constant which is approximately proportional to the $\exp(-\Delta H^{\#}/kT)$, where $\Delta H^{\#}$ is the apparent enthalpy of activation (hereafter simply termed as the activation energy), and k is the Boltzmann constant. The activation energies are evaluated at a fixed overpotential (h) using the Arrhenius equation

$$\frac{\partial(\log i_k)}{\partial(t/T)}\Big|_{\eta} = \frac{\Delta H^*}{2.3R} \qquad (3)$$

The Arrhenius plots at $\eta = 0.3$ V for three different catalysts are shown as an insert in Figure 4. The activation energies determined from the least-squares regressions are essentially identical and range between 20 and 23 kJ/mol; see Table 1. These values are in close agreement with values reported for single-crystal platinum electrodes,[54] polycrystalline platinum,[55] and for carbon-supported Pt[16] in both H_2SO_4 and $HClO_4$ solutions. In a previous study, we reported activation energies between 20 and 25 kJ/mol for carbon-supported Pt_3Ni and Pt_3Co alloys in a comparable potential range in $HClO_4$.[16] One should keep in mind, however, that the assessments of activation energies at the same overpotential is only an estimate of the activation energy, i.e., $\Delta H^{\#}$ is the "apparent" activation energy. Kinetic currents (i_k in eq 3) are strongly dependent on the amount of "oxide" on the Pt surface[56] which, in turn, is temperature-dependent. Even though the oxide coverage is a preexponential term in eq 6, it is a temperature-dependent quantity.

As for activation energies, the Tafel slope obtained for the Pt_3Ni, Pt_3Co, and "Pt-skin" bimetallic surfaces is almost the same as for the pure Pt, (see Table 1). Inspection of Table 1 reveals two important differences between the Tafel slopes for the ORR in $HClO_4$ versus H_2SO_4 on all surfaces. (i) While a single linear Tafel slope was obtained in H_2SO_4,[64] two Tafel slopes can be extrapolated in $HClO_4$. (ii) While in H_2SO_4 the Tafel plots are directly proportional to the temperature, in $HClO_4$ the Tafel plots are inversely proportional to the temperature. Very recently, we found that if the oxide formation on Pt (*hkl*) is controlled rather with strongly adsorbing anions of supporting electrolytes (e.g., Br^-, HSO_4^-) than with temperature of electrolytes, then the $i-E$ relationship has an ideally temperature-dependent Tafel slope ($-2 \times 2.3(RT/F)$).[49,54] On the other hand, it was demonstrated that when temperature plays an important role in the oxide formation on Pt(*hkl*), e.g., as in alkaline solutions, then the $\partial(\log i)/\partial E$ relationship is inversely proportional to the RT/F term.[56] Hence, in H_2SO_4 electrolyte the $i-E$ relationship is in good agreement with a classical electrochemical kinetic theory[57] which predicts that the Tafel slope should be directly proportional to the temperature. In $HClO_4$, however, decreasing of the "apparent" Tafel slopes with increasing temperature on all electrodes may indicate that the $\partial(\log i)/\partial E$ contains a significant contribution from the temperature dependence of oxide formation on these electrodes as found for the ORR on Pt(*hkl*) in alkaline solutions.[56]

3.4. Reaction Pathway. The fact that essentially the same kinetic parameters are assessed from the analysis of experimental results for the ORR on all three surfaces implies that the reaction mechanism on Pt_3Ni and Pt_3Co alloy surfaces is the *same* as one proposed for pure Pt, i.e., a "series" $4e^-$ reduction pathway which can be presented schematically as[49,54,58] The first step in

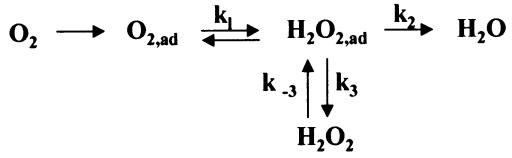

the overall reaction path is the adsorption of O_2 on the Pt surface,

$$O_2 \rightarrow O_{2(ad)} \tag{4}$$

which is followed by the rate-determining step[65]

$$O_{2(ad)} + e^- \rightarrow O^-_{2(ad)} \tag{5}$$

If the rate-controlling step is the first charge transfer in eq 5 then, for the first-order dependence of the kinetics of the ORR found in this work, the general rate expression can be given by eq 6:[49]

$$i = nFKC_{O_2}(1 - m\Theta_{ad})^x \exp(-\beta FE/RT) \exp(-\gamma r\Theta_{ad})/RT) \tag{6}$$

where n is the number of electrons, K is the rate constant, C_{O_2} is the concentration of O_2 in the solution, Θ_{ad} is the total surface coverage by adsorbed species (hydroxyl and bisulfate anions), x is the order of active Pt sites, $m = 1$ is the number of Pt sites blocked by OH_{ad}, i is the observed current, E is the applied potential, β and γ are the symmetry factors (assumed to be $^1/_2$), $r\Theta_{ad}$ is a parameter characterizing the rate of change of the apparent standard free energy of adsorption with the surface coverage by adsorbing species, T is temperature, F is Faraday's constant, and R is the universal gas constant. A number of theories have been proposed to explain the transition in the Tafel slope on the polycrystalline Pt electrode, i.e., to the change from Temkin to Langmuirian conditions for the adsorption of reaction intermediates,[59−61] or as being due to a change in the surface coverage by OH_{ad} and specifically adsorbing anions which control the availability of the adsorption of molecular O_2.[45,46] Very recently, on the basis of eq 4, a theoretical model was developed which showed that in $HClO_4$ the best fit of the $i-E$ relationship can be obtained by implying both blocking and energetic components.[49] In H_2SO_4, however, the energetic effect is of minor importance because the adsorption of reaction intermediates which are formed during the ORR occurs under Langmuirian conditions.[49,54] Consequently, in H_2SO_4 the rate of the ORR may be correlated only with the availability of free Pt sites for the adsorption of reactants and intermediates, i.e., the $(1 - \Theta_{ad})$ term. Closely following these arguments and based on the facts that Pt and Pt-alloys have the same Tafel slopes in both electrolytes, one may suggest that in $HClO_4$ the Tafel slopes for the ORR on the Pt_3-Ni, Pt_3-Co, and "Pt-skin" alloys are controlled by both energetic and blocking effects. In H_2SO_4, however, the rate of the ORR is predominantly determined by the surface coverage of bisulfate anions (blocking effects).

In previous studies,[9−15] the principal explanation for the enhanced ORR activity on Pt−Ni and Pt−Co alloys was enumerated as being a result of one or more of the following effects: (i) modification of the electronic structure of Pt (5-d orbital vacancies); (ii) change in the physical structure of Pt (Pt−Pt bond distance and coordination number); (iii) adsorption of oxygen-containing species from the electrolyte onto the Pt or alloying element; and/or (iv) redox-type processes involving the first-row transition alloying elements.

Our results for the Pt_3Ni and Pt_3Co alloys suggest that, because the (chemical) rate constant K and the two exponential terms are essentially identical for all three systems, the ORR kinetics on these three surfaces is predominantly controlled by the $(1 - \Theta_{ad})$ term. As discussed in ref 5, in H_2SO_4 the $(1 - \Theta_{ad})$ term is mainly determined by the potential-dependent specific adsorption of bisulfate anions. In $HClO_4$, however, the $(1 - \Theta_{ad})$ term is primarily determined with the potential-dependent surface coverage of OH_{ad} species.[49] As one can see from Figure 6c, the catalytic effect of this term is ca. 1.5−4 vs pure Pt, which is consistent with the shift of ca. 50 mV in oxidation potential. We do not have a definitive explanation why Ni and Co in the Pt surface would cause either the decrease in the surface coverage by bisulfate anions or induce the positive shift in the oxidation potential of the Pt surface. In fact, a decrease in anion adsorption is just opposite what would one expect on the basis of the change of the local potential of zero charge (pzc) of Pt atoms neighbored by Ni(Co). Notice that alloying Pt with less noble metals lowers the work function (pzc) of the Pt surface and Pt atoms near the alloying elements (Ni,Co) have a positive charge with respect to Pt atoms far away,[62] resulting in enhanced anion adsorption at these sites at a given electrode potential. The magnitude of the lowering of the pzc will depend on the state of the charge of alloying elements and other details of the Pt−Ni(Co) interaction, i.e., the local dipole moment. Although hypothetical, we offer some plausible explanation arguing that the local pzc concept might not be so important in controlling the adsorption of anions and oxide formation on the Pt−Ni(Co) surface. In particular, for specific adsorption of anions, one may argue that the interaction of tetrahedral bisulfate anions is hindered on alloy surfaces as a result of lack of ensemble of Pt atoms required for $Pt-HSO_4^-$ interaction. Notice that Ni and Co are oxidized and therefore these sites are inactive for adsorption of bisulfate anions. In the case of Pt−OH, one may hypothesize that the adsorption of OH_{ad} *on* the Pt sites is modified as a result of mutual interaction between OH_{ad} and "oxide"-covered Ni and Co atoms beyond 0.8 V. As for Pt−O interaction in UHV, the isosteric heat of adsorption of OH_{ad} on Pt sites (the surface coverage) surrounded by "oxide"-covered Ni and Co atoms may be reduced significantly primarily from lateral repulsive interactions, and to a much lesser extent the occupation of different adsorption sites. Therefore, being oxidized at much lower potentials than Pt, it appears that Ni and Co atoms may serve as "sacrificial" elements in Pt−Ni and Pt−Co alloys.

Figure 6 shows that, interestingly, the "Pt-skin" electrode has a uniquely high catalytic activity for the ORR in $HClO_4$. The rate of the ORR on the "Pt-skin" is increased by a factor of 4 relative to a pure Pt electrode. Very recently, a significant enhancement in the rate of the ORR in KOH was observed on a pseudomorphic monolayer film of Pd[63] grown epitaxially on Pt(111). The monolayer film is about 5 times more active than the Pd multilayer, even though the latter is a rougher surface. In this study it was proposed that the enhanced catalytic activity of the Pt(111)−Pd surface vs the Pt(111) surface arises as a result of modification of surface electronic properties caused by charge redistribution upon forming the Pt−Pd bond. The same argument can be used in this system for the "Pt-skin" which is formed over the Pt-depleted second layer, e.g., as a

result of the change of electronic structure the nature of oxide formation on the "Pt-skin" is changed, causing the reduction of surface oxide to take place at more positive potentials. Theoretical aspects of the relationships between the electronic structure and reactivity are, however, required in order to understand the trends in atomic/molecular chemisorption energies of oxygen-containing species on the Pt_3Ni, Pt_3Co, and "Pt-skin" bimetallic surfaces.

4. Conclusions

The intrinsic catalytic activity of Pt_3Ni and Pt_3Co alloy catalysts for the ORR are studied on UHV-prepared (annealing/sputtering cycles) and characterized (AES and LEIS) alloys in acid electrolytes. Polycrystalline bulk alloys of Pt_3Ni and Pt_3Co can be prepared in UHV having two different surface compositions: one with 75% Pt and the other with 100% Pt. The latter we called a "Pt-skin" structure and is produced by an exchange of Pt and Co in the first layers. The base voltammetry in 0.1 M $HClO_4$ solution of the 75% Pt alloy surface indicated a decrease of H_{upd} pseudocapacitance (ca. 30−50 $\mu C/cm^2$) consistent with the surface composition determined by LEIS. Surprisingly, a decrease of H_{upd} pseudocapacitance was also observed on the "Pt-skin" electrode, consistent with the electronic effect of intermetallic bonding of the Ni(Co)-rich second layer with the topmost Pt atoms. Activities of Pt-alloys for the ORR were compared to the polycrystalline Pt in 0.5 M H_2SO_4 and 0.1 M $HClO_4$ electrolytes in the temperature range of $298 < T < 333$ K. With the exception of the "Pt-skin" surface on P_3Ni, all the alloy electrodes exhibited stable $i-E$ curves with repeated cycling between 0.05 and 1.0 V at all temperatures. It was found that the order of activity is strongly dependent on the nature of anions of supporting electrolytes: in H_2SO_4 the activity decreased in the order $Pt_3Ni > Pt_3Co > Pt$; in $HClO_4$, however, the order of activities at 333 K was "Pt-skin"$> Pt_3Co > Pt_3Ni > Pt$. The catalytic enhancement was greater in 0.1 M $HClO_4$ than in 0.5 M H_2SO_4, with the maximum enhancement observed for the "Pt-skin" on Pt_3Co in 0.1 M $HClO_4$ being 3−4 times that for pure Pt. Kinetic analyses of RRDE data revealed that kinetic parameters for the ORR and the production of H_2O_2 on the Pt_3Ni, Pt_3Co, and "Pt-skin" alloys are the same as on pure Pt: the reaction order, $m = 1$, two identical Tafel slopes in $HClO_4$, and a single Tafel slope in H_2SO_4, the "apparent" activation energy, $\approx$ 20−25 kJ/mol. The fact that essentially the same kinetic parameters are assessed from the analysis of experimental results for the ORR on all three surfaces implies that the reaction mechanism on Pt_3Ni and Pt_3Co alloy surfaces is the *same* as the one proposed for pure Pt, i.e., a "series" $4e^-$ reduction pathway. Catalytic enhancement of the ORR on Pt_3Ni and Pt_3Co vs Pt was attributed to the inhibition of $Pt-OH_{ad}$ formation *on* Pt sites surrounded by "oxide"-covered Ni and Co atoms beyond 0.8 V. We proposed that catalytic improvement for the "Pt-skin" is caused by electronically modified Pt atoms on the top of the Co-enriched layer underneath. Those findings confirm unique properties of monolayer thin films and thus can be essential in the future design of high-surface-area catalysts for the fuel cells.

Acknowledgment. U. A. Paulus is greatly acknowledged for her contribution to some ORR measurements. This work was supported by the Assistant Secretary for Energy Efficiency and Renewable Energy, Office of Advance Transportation Technologies of the U.S. Department of Energy under Contract DE-AC03-76SF00098.

References and Notes

(1) Markovic, N. M.; Ross, P. N. *Surf. Sci. Rep.* **2002**, *286*, 1−113.
(2) EL Kadiri, F.; Faure, R.; Durand, R. *J. Electroanal. Chem.* **1991**, *301*, 177−188.
(3) Markovic, N. M.; Gasteiger, H. A.; Ross, P. N. *J. Phys. Chem.* **1995**, *99*, 3411−3415.
(4) Markovic, N. M.; Gasteiger, H. A.; Ross, P. N. *J. Phys. Chem.* **1996**, *100*, 6715−6721.
(5) Markovic N. M.; Ross, P. N., Jr. *Interfacial Electrochemistry−Theory, Experiments and Applications*; Wieckowski, A., Ed.; Marcel Dekker Inc.: New York, 1999; Chapter 46, pp 821−841.
(6) Climent, V.; Markovic, N. M.; Ross, P. N. *J. Phys. Chem. B* **2000**, *104*, 3116−3120.
(7) Markovic, N. M.; Lucas, C.; Climent, V.; Stamenkovic, V.; Ross, P. N. *Surf. Sci.* **2000**, *465*, 103−114.
(8) Appleby, A. J. *Catal. Rev.* **1970**, *4*, 221−244.
(9) Luczak, F. J.; Landsman, D. A. Ordered Ternary Fuel Cell Catalysts Containing Platinum, Cobalt and Chromium. U.S. Patent 4,447,506, 1984.
(10) Lucas, C. A.; Markovic, N. M.; Ross, P. N. *Phys. Rev. B* **1997**, *55*, 7964−7971.
(11) Luczak, F. J.; Landsman, D. A. Ordered Ternary Fuel Cell Catalysts Containing Platinum and Cobalt and Method for Making the Catalyst. U.S Patent 4,677,092, 1987.
(12) Beard, B.; Ross, P. N. Jr. *J. Electrochem. Soc.* **1990**, *137*, 3368.
(13) Glass, J. T.; Cahen, G. L.; Stoner, G. E. *J. Electrochem. Soc.* **1987**, *134*, 58.
(14) Mukerjee, S.; Srinivasan, S. *J. Electroanal. Chem.* **1993**, 201.
(15) Toda, T.; Igarashi, H.; Uchida, H.; Watanabe, M. *J. Electrochem. Soc.* **1999**, *141*, 968.
(16) Paulus, U. A.; Scherer, G. G.; Wokaun, A.; Schmidt, T. J.; Stamenkovic, V.; Radmilovic, V.; Markovic, N. M.; Ross, P. N. *J. Phys. Chem. B* **2001**, *106*, 4181−4191.
(17) Markovic, N. M.; Schmidt, T. J.; Stamenkovic, V.; Ross, P. N. *Fuel Cells−From fundamentals to stems* **2001**, *2001*, 105−116.
(18) Bardi, U.; Beard, B.; Ross, P. N. *J. Catal.* **1990**, *124*, 22.
(19) Ross, P. N. *Electrocatalysis*; Lipkowski, J., Ross, P. N., Eds.; Wiley-VCH, Inc.: New York, 1998; Chapter 2, pp 43−74.
(20) Gasteiger, H. A.; Markovic, N.; Ross, P. N. *J. Phys. Chem.* **1995**, *99*, 16757−16767.
(21) Gasteiger, H. A.; Markovic, N. M.; Ross P. N., Jr. *Catal. Lett.* **1996**, *36*, 1−8.
(22) Strohl, J. K.; King, T. S. *J. Catal.* **1989**, *116*, 540.
(23) Markovic, N. M.; Ross, P. N. *Electrochim. Acta* **2000**, *45*, 4101−4115.
(24) Vasiliev, M. A. *J. Phys. D: Appl. Phys.* **1997**, *30*, 3037−3070.
(25) Watson, P. R; Van Hove, M. A.; Herman, K. Atlas of surface stucture. [Volume IA, Monograph 5]. American Chemical Society: Washington, DC, 1995.
(26) Gasteiger, H. A.; Markovic, N.; Ross, P. N.; Cairns, E. J. *J. Phys. Chem.* **1993**, *97*, 12020−12029.
(27) Markovic, N. M.; Grgur, B. N.; Ross, P. N., Jr. *J. Phys. Chem. B* **1997**, *101*, 5405−5413.
(28) Sachtler, W. M. H.; van Santen, R. A. *Adv. Catal.* **1977**, *26*, 69.
(29) Chelikowski, J. R. *Surf. Sci.* **1984**, *139*, L197.
(30) Campbell, C. T. *Annu. Rev. Phys. Chem.* **1990**, *41*, 775−837.
(31) Dowben, A. P.; Miller, A. *Surface segregation phenomena*; CRC Press: Boca Raton, FL, 1990.
(32) Polak, M.; Rubinovich, L. *Surf. Sci. Rep.* **1999**, *262*, 1−68.
(33) Kuntze, J.; Speller, S.; Heiland, W.; Atrei, A.; Rovida, G.; Bardi, U. *Phys. Rev. B* **1999**, *60*, 1535−1538.
(34) Kuntze, J.; Speller, S.; Heiland, W.; Deurinck, P.; Creemers, C.; Atrei, A.; Bardi, U. *Phys. Rev. B* **1999**, *60*, 9010−9018.
(35) Niehus, H. *Phys. Status Solidi B* **1995**, *192*, 357.
(36) Gauthier, Y.; Baudoing, R.; Rundgren, J. *Phys. Rev. B* **1985**, *31*, 6216−6218.
(37) Bardi, U.; Atrei, A.; Zanazzi, E.; Rovida, G.; Ross P. N., Jr. *Vacuum* **1990**, *41*, 437−440.
(38) Gauthier, Y. *Surf. Rev. Lett.* **2001**, *3*, 1663−1689.
(39) Smith, D. P. *J. Appl. Phys.* **1967**, *38*, 340−347.
(40) Taglauer, E. *Appl. Phys. A* **1985**, *38*, 161−170.
(41) Paredes Olivera, P.; Patrito, M. *Interfacial Electrochemistry, Theory, Experiment, and Applications*; Wieckowski, A., Ed.; Marcel Dekker: New York, Basel, 1999; Chapter 5, pp 63−81.
(42) Jerkiewicz, G. *Prog. Surf. Sci.* **1998**, *57*, 137−186.
(43) Markovic, N. M.; Schmidt, T. J.; Grgur, B. N.; Gasteiger, H. A.; Ross, P. N., Jr.; Behm, R. J. *J. Phys. Chem. B* **1999**, *103*, 8568−8577.
(44) Schmidt, T. J.; Paulus, U. A.; Gasteiger, H. A.; Alonso-Vante, N.; Behm, R. J. *J. Electrochem. Soc.* **1999**.
(45) Tarasevich, M. R. *Electrochimiya* **1973**, *9*, 578.
(46) Tarasevich, M. R.; Vilinskaya, V. S. *Electrochimiya* **1973**, *9*, 96.

(47) Uribe, F.; Wilson, M. S.; Springer, T.; Gottesfeld, S. Oxygen Reduction (ORR) at the Pt/Recast Ionomer Interface and Some General Comments on the ORR at Pt/Aqueous Electrolyte Interfaces. *Proceedings of the Workshop on Structural Effects in Electrocatalysis and Oxygen Electrochemistry*, Cleveland, OH, October, 1991; Scherson, D., Tryk, D., Daroux, M., Xing, X., Eds.; Electrochem. Soc., Vol. 92−11, p 494.

(48) Adzic, R. R. Surface Morphology Effects in Oxygen Electrochemistry. *Proceedings of the Workshop on Structural Effects in Electrocatalysis and Oxygen Electrochemistry*, Cleveland, OH, October, 1991; Scherson, D., Tryk, D., Daroux, M., Xing, X., Eds.; Electrochem. Soc., Vol. 92−11, p 419.

(49) Markovic, N. M.; Gasteiger, H. A.; Grgur, B. N.; Ross, P. N. *J. Electroanal. Chem.* **1999**, *467*, 157−163.

(50) Albery, W. J.; Hitchman, M. L. *Ring-Disc Electrodes*; Clarendon Press: Oxford, 1971.

(51) *CRC Handbook of Chemistry and Physics*, 66th ed.; CRC Press: Boca Raton, FL, 1986.

(52) Schumpe, A.; Adler, I.; Deckwer, W.-D. *Biotechnol. Bioeng.* **1978**, *20*, 145.

(53) Anastasijevic, N. A.; Dimitrijevic, Z. M.; Adzic, R. R. *Electrochim. Acta* **1986**, *31*, 1125−1130.

(54) Grgur, B. N.; Markovic, N. M.; Ross, P. N., Jr. *Can. J. Chem.* **1997**, *75*, 1465−1471.

(55) Damjanovic, A.; Sepa, D. B. *Electrochim. Acta* **1990**, *35*, 1157−1162.

(56) Schmidt, T. J.; Stamenkovic, V.; Arenz, M.; Markovic, N. M.; Ross, P. N. *Electrochim. Acta* **2002**, *1*, 1.

(57) Vetter, K. J. *Electrochemical Kinetics*; Academic Press: New York, 1967.

(58) Stamenkovic, V.; Markovic, N. M.; Ross, P. N., Jr. *J. Electroanal. Chem.* **2000**, *500*, 44−51.

(59) Damjanovic, A.; Genshaw, M. A.; Bockris, J. O. M. *J. Phys. Chem.* **2001**, *45*, 4057.

(60) Damjanovic, A. *Modern Aspects of Electrochemistry*; Plenum Press: New York, 1969; Chapter 5, pp 369−483.

(61) Tarasevich M. R.; Sadkowski, A.; Yeager, E. *Comprehensive Treatise in Electrochemistry*; Plenum Press: New York, 1983; Chapter 6, pp 301−398.

(62) Markovic, N. M.; Ross, P. N. *J. Electroanal. Chem.* **1992**, *330*, 499−520.

(63) Arenz, M.; Wandelt, K.; Stamenkovic, V.; Schmidt, T. J.; Ross, P. N., Jr.; Markovic, N. M. *J. Phys. Chem.*, to be published.

(64) The number of data points in the "low current density" potential region is relatively small in H_2SO_4 and barely more than the minimum of three points to determine the slope.

(65) It has been proposed that the rate-determining step for the ORR on the Pt(111) surface in pure perchloric acid is also the first charge-transfer step although the Tafel slope was different from 120 mV dec^{-1}.[49]